**Tissue engineering a surrogate niche for metastatic cancer cells**

F. Philipp Seib[a,1], Janice E. Berry[b], Yusuke Shiozawa[b], Russell S. Taichman[b], David L. Kaplan[a,*]

(a) Tufts University, Department of Biomedical Engineering, 4 Colby Street Medford, MA 02155, USA. (b) Department of Periodontics and Oral Medicine, University of Michigan School of Dentistry, Ann Arbor, Michigan 48109, USA.

(1) Current address: Strathclyde Institute of Pharmacy and Biomedical Sciences, University of Strathclyde, 161 Cathedral Street, Glasgow, G4 0RE, UK

(*) Corresponding author: David L. Kaplan; Tel: +1 617-627-3251; Fax: + 1 617-627-3231; email: David.Kaplan@tufts.edu

**Running title:** Tissue-engineered cancer trap

**Abstract**

In breast and prostate cancer patients, the bone marrow is a preferred site of metastasis. We hypothesized that we could use tissue-engineering strategies to lure metastasizing cancer cells to tissue-engineered bone marrow. First, we generated highly porous 3D silk scaffolds that were biocompatible and amenable to bone morphogenetic protein 2 functionalization. Control and functionalized silk scaffolds were subcutaneously implanted in mice and bone marrow development was followed. Only functionalized scaffolds developed cancellous bone and red bone marrow, which appeared as early as two weeks post-implantation and further developed over the 16-week study period. This tissue-engineered bone marrow microenvironment could be readily manipulated *in situ* to understand the biology of bone metastasis. To test the ability of functionalized scaffolds to serve as a surrogate niche for metastasis, human breast cancer cells were injected into the mammary fat pads of mice. The treatment of animals with scaffolds had no significant effect on primary tumor growth. However, extensive metastasis was observed in functionalized scaffolds, and the highest levels for scaffolds that were *in situ* manipulated with receptor activator of nuclear factor kappa-B ligand (RANKL). We also applied this tissue-engineered bone marrow model in a prostate cancer and experimental metastasis setting. In summary, we were able to use tissue-engineered bone marrow to serve as a target or "trap" for metastasizing cancer cells.

**Key words:** bone, silk, cancer, metastasis, breast cancer, microenvironment

## Introduction

Metastasis is a highly complex process. In the case of breast and prostate cancers, hematogeneous metastasis is commonly encountered in the red bone marrow [1], and patient survival is poor once disseminated disease is diagnosed [2]; metastasis is responsible for 90% mortality of patients with solid tumors [3]. The lack of suitable *in vivo* tissue models has impeded clinical progress [4]. There are currently two main approaches for studying syngeneic or xenograft breast and prostate cancer bone metastasis in the orthotopic or experimental metastasis setting [5]. In the first, the host's skeleton serves as the site of metastasis and is commonly used to study osteotropism of cancer. In the second, fresh bone chips [6-9] or marrow [10] are used and implanted subcutaneously or in the mammary fat pad. While human fetal bone or marrow has been used in most cases [6, 8], materials from discarded femoral heads [9] have also been used.

Tissue-engineering approaches for cancer research [11] have recently emerged as a potential third route for the study of bone metastasis. For example, microfabricated scaffolds seeded with human bone marrow stromal cells have been implanted in a window chamber model to permit intravital microscopy studies [12]. This microfabricated model generated a chimeric microenvironment, but the ability of this model to recapitulate native tissue remains to be established. Bone marrow stromal cells are clearly useful for driving osteogenesis and marrow formation [13]; however, bone morphogenetic proteins (BMPs) also have a robust clinical track record for the *de novo* formation of bone and marrow [14]. In particular, BMP-2 has been associated with bone development and maintenance in the adult skeleton [14, 15]. *In vivo* tissue engineering of bone has been successful [16], but no attempts have yet been made to engineer a bone marrow microenvironment (BMM) that can be selectively manipulated. This manipulation of the BMM would provide opportunities to ask fundamental questions about cancer metastasis to bones, and to explore the possibility that tissue-engineered bone could serve as a surrogate niche or "trap" for cancer metastasis. Several

potential avenues are available for manipulating the BMM; chemokines were chosen in the present study.

In 1889, Stephen Paget established that breast cancer has preferred sites for metastasis (tissue tropism) [17], and recent studies have identified chemokines as potential regulators that dictate the actual organ metastasis of breast [18] and prostate [19] cancers (reviewed in [20, 21]). For example, metastatic breast and prostate cancers "home" to bone by following gradients of stromal cell-derived factor 1 (SDF-1); this mechanism emulates the hematopoietic stem trafficking occurring during fetal development and following bone marrow transplantation [20].

Bone colonization by metastatic cancer cells involves the hijacking of a multitude of signaling pathways [22]. For example, osteotropic cancers often induce osteoclast activity through receptor activator of nuclear factor kappa-B ligand (RANKL) signaling. Osteoclast activation in the BMM in turn liberates a myriad of growth factors and chemokines stored in the bone mineral matrix, thereby driving the recruitment of even more cancer cells to the bone [2, 22]. Our current understanding of chemokine-mediated metastasis indicated SDF-1 and RANKL as appropriate choices for manipulation of the BMM in the present study.

In summary, this study examined the potential of BMP-2 functionalized scaffolds to support the *in vivo* development of bone and marrow and the subsequent ability of this tissue-engineered BMM to serve as a surrogate niche for metastatic cancer cells attracted by locally released chemokines.

## Materials and Methods

**Preparation of silk scaffolds.** *Bombyx mori* silk solution was prepared as described previously [23]. Briefly, cocoons were cut into 25-$mm^2$ pieces, boiled for 30 min in an aqueous solution of 25 mM $Na_2CO_3$, and then rinsed in distilled $H_2O$ to remove sericin proteins. Extracted silk fibroin was

subsequently air dried and then dissolved in 9.3 M LiBr solution at 60°C for 4 h, yielding a 25% w/v solution. This solution was dialyzed against $ddH_2O$ (molecular weight cut off 3500) for 48 h to remove the LiBr salt. The resulting aqueous silk fibroin solution was centrifuged twice at 9.700 g for 20 min to remove the small amount of silk aggregates that formed during processing. A salt-leach method was used where NaCl crystals were embedded within silk fibroin to generate highly porous silk scaffolds. First, the silk fibroin solution was diluted to 6% w/v with $ddH_2O$. Next, 4 g of NaCl crystals (500–600 μm) were added to 2 ml of this fibroin solution as porogens, and scaffolds were allowed to solidify for 24 h. Scaffolds were washed extensively in $ddH_2O$ to leach out the NaCl to yield highly porous silk scaffolds. The size was optimized by generating scaffolds with a volume of either 125 $mm^3$ or 27 $mm^3$ and a constant 5 μg BMP-2 (human BMP-2, Wyeth, Andover, MA, USA) loading. For 125 $mm^3$ scaffolds, BMP-2 loading was optimized using BMP-2 concentrations between 0.5 and 10 μg. For all samples, the BMP-2 loading was performed by applying 30 μl of a 7% w/v silk solution containing the indicated amount of BMP-2. Scaffolds were air dried under a 0.2-m/s airflow at room temperature overnight. Where indicated, scaffolds were further modified by water annealing at room temperature for 8 h to induce β-sheets [23].

***In vivo* scaffold implantation.** Animal studies were performed in accordance with the approved institutional protocols B2010–101 and PRO00004354 by the Institutional Animal Care and Use Committee (IACUC) of Tufts University and University of Michigan, respectively. Mice aged 6 to 10 weeks were purchased from Charles River Laboratories. For scaffold implantation studies, animals were anesthetized using isoflurane, shaved when necessary, and the surgical area was cleaned. As indicated, BMP-2 functionalized or control silk scaffolds were implanted subcutaneously at three different sites, namely the rotator cuff, lower abdomen, and upper thorax. As controls, 10 mg of demineralized human (0.125–0.850 mm particle size; Community Tissue Services, Dayton, OH, USA) or rat bone were added to a size 9 gelatin capsule (Torpac Inc., Fairfield, NJ, USA) and implanted as detailed above. Incisions were closed with a one-layer closure

using skin clips. Animals were monitored daily over the course of 10 days, at which time the skin clips were removed. Scaffolds were removed at the indicated time points and processed for analysis as detailed below.

**Cell culture.** All cell lines were maintained in a humidified atmosphere of 5% $CO_2$ at 37°C, and subconfluent cultures were routinely subcultured every 2–3 days. The following media were used: MDA-MB-231 and B16F10 cells, RPMI 1640 + 10% v/v FBS; PC3 cells, RPMI 1640 + 10% v/v FBS. For *in vivo* tumor studies, cells were harvested with trypsin and subsequently prepared as detailed below.

**Tumor models.** To examine the potential of tissue-engineered bone to serve as a surrogate niche to cancer metastasis, a syngeneic experimental tumor model employing C57BL/6 mice and B16F10 cancer cells was used [24]. Prior to tumor cell injection, a 125-$mm^3$ scaffold functionalized with 5 μg BMP-2 was implanted over the rotator cuff in mice and allowed to integrate for more than 4 weeks. On the day of tumor induction, B16F10 cells were washed and harvested with trypsin-EDTA, blocked with complete medium, and pelleted. The pellet was subsequently washed twice with PBS, and cells were resuspended in PBS at a concentration of $10^5$ cells/ml and kept on ice. Mice were shaved, cleaned and the landmarks palpitated to facilitate the intracardiac injection of cells into the left ventricle. The spontaneous pulsatile entrance of bright red oxygenated blood into the transparent needle hub indicated proper positioning of the needle. A dose of $10^4$ B16F10 cells in 100 μl was administered over 30 s into the left ventricle with a 27-gauge needle. Within 18 days of B16F10 injection, animals were euthanized.

For studies that examined the potential of the scaffolds to serve as a surrogate niche for breast cancer metastasis, a human xenograft model was used. Breast tumors were induced by inoculating MDA-MB-231 derived tumor cells that metastasized following orthotopic injection in mice [25].

Cells were genetically modified to carry the firefly luciferase gene to allow *in vivo* bioluminescence imaging [25]. Analogous to the syngeneic tumor studies, scaffolds were implanted over the rotator cuff in female NOD/SCID mice (NOD.CB17-Prkd$^{scid}$/NcrCrl), 6–10 weeks in age, and allowed to integrate ≥8 weeks. Next, a total of $5\times10^5$ cells in 20 µl Matrigel (BD Biosciences, Bedford, MA, USA) was injected bilaterally into the 4$^{th}$ or 5$^{th}$ mammary fat pad using a Hamilton syringe equipped with a 22-gauge needle. To manipulate the microenvironment of the tissue-engineered bone, osmotic minipumps (Durect Corporation, Cupertino, CA, USA) were used. Pumps with a nominal pumping rate of 0.11 µl/h over 4 weeks were fitted with an infusion catheter and filled with SDF-1 (100 µg/ml), RANKL (100 µg/ml), or PBS according to the manufacturer's instruction; human SDF-1 alpha (catalogue number 100-20) and mouse RANKL (catalogue number 200-04) were purchased from Shenandoah Biotechnology, Warwick, PA, USA. Twelve days after tumor inoculation, pumps were implanted s.c. and the catheter was implanted into the scaffold. Disease progression was monitored weekly with intraperitoneal injections of D-luciferin (Molecular Probes, Eugene, OR, USA), followed by measuring tumor cell-associated bioluminescence using the Xenogen IVIS 200 imaging system and Living Image Software 4.2 (Caliper Life Sciences, Hopkinton USA). At the study endpoint at 6 weeks post-tumor induction, scaffolds, brain, lung, liver, and bones were examined for metastasis by dissecting them from the carcass. Tibia and femur from hind legs were harvested and dissected free from muscle and tendons to serve as bone samples. Organs were imaged at maximum sensitivity to detect metastatic cancer cells. Tissues were scored for the presence or absence of metastasis. Primary tumors were dissected and weighed.

For prostate cancer studies, one scaffold was implanted on the back of male athymic nude mice (Athymic Nude-*Foxn1*$^{nu}$), 6–10 weeks in age, and allowed to integrate >6 weeks. PC3 cells were transduced with GFP-luciferase lentivirus to allow for bioluminescence imaging of tumor growth (via luciferase) and localization of cells in tissue sections (via GFP). Next, a total of $1\times10^5$ cells in 10 µl growth medium was injected into the ossified scaffold with a 30-gauge needle. At the time of

cell injection, a single pump with either SDF-1 or PBS was implanted as detailed above.

**Histology and X-ray microtomography**. X-ray microtomography was performed on formalin-fixed tissues in 70% v/v ethanol. Measurements were carried out with an HMX ST 225 X-ray tube equipped with a molybdenum target and a 2000×2000 pixel detector (Nikon Metrology, Leuven, Belgium). Projections were recorded over 360°, and dataset voxel sizes were typically 10 μm isotropic. The data set was reconstruction with the CTPro 3D software package (Nikon Metrology) in the absence of noise reduction or binning. Images were rendered using VGStudio MAX version 2.2 (Volume Graphics, Heidelberg, Germany).

Bones and scaffolds were prepared for histology by fixing them for 24 h in buffered formalin and subsequently demineralizing them for 21 days at 4°C with a 10% w/v EDTA solution at pH 7.4. Next, samples were tissue processed and paraffin embedded as detailed previously [26]. For all histology samples, at least two level sections were cut to ensure representative images. For immunofluorescence images to detect human cells grown in scaffolds, anti-human HLA-ABC antibody (BioLegend) was conjugated using the Zenon Alexa Fluor488 mouse IgG labeling kit (Invitrogen, San Diego, CA). Seven $\mu$m thick paraffin sections were blocked with Image-iT FX signal enhancer (Invitrogen) for 30 min before fluorescence-labeled and primary antibodies were applied for 2 h at room temperature in the dark. Subsequently, the sections were mounted with ProLong Gold anti-fade reagent with DAPI (Invitrogen). Images were taken with Olympus FV-500 confocal microscope (Olympus, Center Valley, PA).

**Statistical analysis**. Data were analyzed using GraphPad Instat 5.0b (GraphPad Software, La Jolla, CA, USA). Sample pairs were analyzed with the Student's *t*-test. Multiple samples were evaluated by one-way analysis of variance followed by Dunnett's post hoc tests to evaluate the statistical differences ($p \leq 0.05$) between samples and controls, respectively. An exception was the analysis of

explanted scaffolds where a Kruskal-Wallis test was used. All error bars were standard deviation (SD).

**Results**

Here we describe an *in vivo* tissue-engineered bone marrow model that uses bone morphogenetic protein 2 (BMP-2) functionalized three-dimensional (3D) silk protein scaffolds that permit *in situ* bone marrow genesis. The bone marrow can subsequently be modified with an osmotic mini pump to locally deliver chemokines or other molecules of interest. We used a water-based silk solution to generate 3D scaffolds that were sponge-like (ca. 50 kPa compressive stress), highly porous (>90%) [27], biocompatible [28], and readily functionalized with defined amounts of BMP-2 with known release kinetics [29]. First, we fixed the amount of BMP-2 loading at 5 μg per scaffold and determined the importance of the post-loading treatment in relation to the implantation site and time for bone marrow genesis (Fig. 1a, Supplementary Fig. 1). Scaffolds that had a low β-sheet (crystalline) content performed best; this was independent of the implantation site. The first signs of bone development occurred at 3 days in C57/B6 mice, and a robust tissue-engineered BMM occurred at 4 weeks, while NOD/SCID mice required 8 weeks. In C57/B6, NOD/SCID, and athymic nude mice, the BMM was maintained for several months (>3); the optimized silk scaffold showed a robust tissue engineered BMM (Fig. 1b-d). However, control scaffolds showed neither bone nor marrow development in mice (Supplementary Fig 1e). As a reference or control for our functionalized silk scaffolds, we used human and rat demineralized bone matrix (DBM) [5, 30]. While human DBM showed no signs of bone marrow development, rat-derived DBM required at least 8 weeks to develop some bone marrow *in vivo*. Because BMP-2 scaffolds with a low β-sheet content performed best (Fig. 1b-d), we further characterized these scaffolds by changing scaffold size and the degree of BMP-2 functionalization (Fig. 1e-h). In light of orthotopic breast tumor studies, we selected the rotator cuff as an implantation site to physically separate the tissue-engineered BMM from the primary tumor. X-ray microtomography demonstrated that with 0.5–10

μg BMP-2 the amount of bone significantly increased, while there were no differences between the 5 μg and 10 μg BMP-2 scaffolds (Fig. 1e, f). Furthermore, at 5 μg BMP-2 functionalization, the amount of bone formation was independent of scaffold size but increased over 16 weeks (Fig. 1g, h). The 125 $mm^3$ scaffolds with a 5-μg BMP-2 loading were found to be optimal for this study because the size of the engineered tissue allowed easy access and manipulation with an infusion catheter of the osmotic minipump.

Next, we examined the ability of the tissue-engineered BMM to serve as a surrogate niche for metastasis (Fig. 2a). Using mice with an established BMM, we induced orthotopic breast tumors and subsequently manipulated the BMM by locally delivering receptor activator of nuclear factor kappa-B ligand (RANKL). To rule out the potential systemic impact of this RANKL delivery strategy, we monitored primary tumor growth over 6 weeks, and the extent of metastasis (Fig. 2b-d). There was no significant difference between the control group and mice receiving RANKL in terms of primary tumor growth, tumor weight, and metastasis to distant organs (Fig. 2b-d). However, there was a significant impact on the tissue-engineered BMM as determined by X-ray microtomography (Fig. 2f), but this did not affect the bone volume of the rest of the skeleton (Fig. 2g). The tissue-engineered BMM harbored human breast cancer cells (Fig. 2h, i). Bioluminescence imaging demonstrated that the control scaffold, which did not develop bone marrow, had the lowest signal, whereas substantially higher values were obtained for SDF-1, and significantly higher ones were obtained for the RANKL treatment group (Fig. 2h, i).

Finally, we next assessed the ability of our tissue-engineered BMM to serve as a model system to study prostate cancer bone metastasis. While there was tumor engraftment for all animals (5/5), delivery of SDF-1 substantially reduced PC3 growth when compared to controls (Fig. 3c) but with minimal effects on tissue or bone volume (Fig. 3d). Histology confirmed growth of prostate cancer cells in the BMM (Fig. 3e). To complement the human breast and prostate cancer studies, the

B16F10 syngeneic experimental metastasis model was used (Fig. 3f). Histology of scaffolds demonstrated that B16F10 cells were able to invade and colonize the tissue-engineered BMM (Fig. 3g-j).

**Discussion**

In 1889, Stephen Paget established that breast cancer has preferred sites for metastasis (tissue tropism) [17], and recent studies have identified chemokines as potential regulators that dictate the actual organ metastasis of breast and prostate cancer [3]. We therefore examined the ability of the tissue-engineered BMM to serve as a surrogate niche for metastasis (Fig. 2a). Using mice with an established BMM, we manipulated the BMM by locally delivering receptor activator of nuclear factor kappa-B ligand (RANKL). RANKL activates osteoclasts, which in turn degrade bone and subsequently release growth factors and chemokines stored in the bone matrix [2, 22]; these factors could critically contribute to a pre-metastatic niche. Tumor growth and metastasis was unchanged following local RANKL delivery (Fig. 2b-d); this suggested that RANKL had minimal systemic effects. This was further supported by the observation that RANKL only had a significant impact on the tissue-engineered bone volume (Fig. 2f), but not the bone volume of the rest of the skeleton (Fig. 2g). Most importantly, the tissue-engineered BMM harbored human breast cancer cells (Fig. 2h, i); this colonization could be readily manipulated *in situ*. Bioluminescence imaging demonstrated that the control scaffold, which did not develop bone marrow, had the lowest signal and the highest one was obtained for the RANKL treatment group (Fig. 2h, i). This observation supported our hypothesis that a metastatic niche can be selectively manipulated using tissue engineering. The extent to which this colonization of the BMM recapitulates all steps typically observed in traditional osteotropic cancer models remains to be established. Nonetheless, the idea that metastatic cancer cells exploit a BMM "homing" mechanism analogous to that driving hematopoietic stem trafficking into bone marrow seems quite plausible [20]. We speculate that this

luring of metastatic cancer cells into the BMM would then conceivably reduce the overall metastatic burden in systemic host tissues (Fig. 2d).

We next assessed the ability of our tissue-engineered BMM to serve as a model system to study prostate cancer bone metastasis. Previous *in vitro* and *in vivo* studies showed the significance of the CXCR4/7-SDF-1 signaling axis in tissue tropism for prostate cancer metastasis [21], although direct experimental proof has been difficult to obtain because of a lack of methods that permit the selective manipulation of the BMM. By combining local SDF-1 delivery with prostate cancer cell injection into the tissue-engineered BMM (Fig. 3a, b), it was possible to monitor cell response *in situ*. While there was tumor engraftment for all animals (5/5), delivery of SDF-1 substantially reduced PC3 growth when compared to controls (Fig. 3c) but with minimal effects on tissue or bone volume (Fig. 3d). This observation was unexpected; one might speculate that SDF-1 delivery induced cancer stem cell quiescence [31] resulting in overall reduced metastatic growth. However, additional studies are needed to better understand the underlying biology in the BMM. We currently also do not know how this engineered BMM supports osteoblastic prostate cancer; this is a limitation of the current study.

Current implant-based models for the study of osteotropism of cancers are typically based on fresh bone chips [6, 8, 9] or marrow [10]; these are implanted subcutaneously or into the mammary fat pads of mice. Human fetal bone or marrow has been used in most cases [6, 8], although materials from discarded femoral heads [9] have also been used. These studies are often designed to examine the interaction of human cancer cells with a humanized bone microenvironment; however, a number of limitations arise, as well as logistical and ethical challenges. For example, marrow models are plagued by poor control over the resulting bone microenvironment and by immunological mismatches between the bone marrow-derived immune cells and the human tumor cells (i.e., a potential marrow versus cancer response) (e.g., [10]). Bone chips have additional

limitations and in general show poor vascularization, which often leads to necrosis and subsequent fibrosis [6, 8, 9]. The sharp edges of bone pieces can also often create wound problems or dehiscence in mice. Bone material from orthopedic surgery, in particular, provides little control over the quality of the bone, coupled with a low capacity to sustain hematopoiesis *in vivo* [9].

Humanized bone models are emerging as interesting model systems to study osteotropism of cancer [4]; however, they still require a significant amount of refinement. The current study demonstrates that the use of optimized silk scaffolds resulted in robust vascularization and bone and red marrow development in a syngenic setting, while none of the studied scaffolds showed adverse reactions in mice. This observation is in line with previous *in vivo* studies [32]. We selected silk because it is a biocompatible and biodegradable biopolymer with minimal endogenous biological activity [32, 33]. Here control scaffolds (i.e., silk scaffolds with no BMP-2 functionalization) showed neither bone nor marrow development in mice (Fig 1a). Furthermore these control scaffolds showed the lowest capacity to capture metastatic cancer cells (e.g., Fig. 2h) indicating that at functional bone marrow is critical to lure cancer cells into an tissue-engineered BMM.

Historically, studies examining the BMM have relied on the epiphyses and diaphysis of long bones that are difficult to access and cannot be readily subjected to local manipulation *in situ*. More recently, alternatives have been sought, for example, the calvarium for intravital high-resolution microscopy of the bone marrow [34]. However, local *in situ* manipulation of the calvarium has not been attempted and is expected to be technically challenging. Here, we applied a simple yet powerful method to study osteotropism of breast and prostate cancer cells *in situ*. The benefits of employing a tissue-engineered BMM are twofold. First, it provides a simple and robust method to generate a tissue-engineered BMM *in vivo*. Second, it provides flexibility to manipulate the BMM

with the use of an osmotic minipump. These features will enable future studies of breast and prostate cancer as well as hematopoietic malignancies and bone marrow in general.

## Conclusions

Manipulating the metastatic BMM *in vivo* is technically challenging as current models depend heavily on the host's skeleton, with occasional xenogenic or syngeneic models exploiting either fresh bone chips or the osteogenic properties of whole or fractionated marrow. We developed a simple yet powerful method to *in vivo* tissue engineer a BBM that could be readily manipulated *in situ* to understand the biology of bone metastasis. With the methodology described here, we demonstrated that a tissue-engineered BMM can serve as a surrogate niche for bone marrow metastasis. By selectively manipulating the engineered BMM, it was possible to either increase or suppress the number of metastatic cells at this site.

## Acknowledgments

The authors thank Ilona Konrad for technical assistance. Some of the X-ray microtomography was performed at the Center for Nanoscale Systems (CNS), a member of the National Nanotechnology Infrastructure Network (NNIN), which is supported by the National Science Foundation under NSF award no. ECS-0335765. CNS is part of Harvard University. This research was supported by NIH grant P41 EB002520-05 (Tissue Engineering Resource Center) (DLK), The National Cancer Institute CA093900, CA163124, CA166307 (YS, RST), The Department of Defense W81XWH-11-1-0636 and PC130359 (YS, RST), the Prostate Cancer Foundation (YS, RST), a Mildred Scheel Postdoctoral fellowship from the German Cancer Aid (FPS), and a Marie Curie FP7 Career Integration Grant 334134 within the 7th European Union Framework Program (FPS).

## Author Contribution.

FPS and DLK conceived the study. FPS, JEB, and YS carried out experiments. All authors designed research, discussed the results, and/or advised on the analysis. FPS wrote the manuscript with support from the other authors.

**References**


[1] Weiss L. Comments on hematogenous metastatic patterns in humans as revealed by autopsy. Clin Exp Metastasis 1992;10:191-9.

[2] Coleman RE. Bone cancer in 2011: Prevention and treatment of bone metastases. Nat Rev Clin Oncol 2012;9:76-8.

[3] Gupta GP, Massague J. Cancer metastasis: building a framework. Cell 2006;127:679-95.

[4] Holzapfel BM, Thibaudeau L, Hesami P, Taubenberger A, Holzapfel NP, Mayer-Wagner S, et al. Humanised xenograft models of bone metastasis revisited: novel insights into species-specific mechanisms of cancer cell osteotropism. Cancer Metastasis Rev 2013;32:129-45.

[5] Pettway GJ, McCauley LK. Ossicle and vossicle implant model systems. Methods Mol Biol 2008;455:101-10.

[6] Kyoizumi S, Baum CM, Kaneshima H, McCune JM, Yee EJ, Namikawa R. Implantation and maintenance of functional human bone marrow in SCID-hu mice. Blood 1992;79:1704-11.

[7] Nemeth JA, Harb JF, Barroso U, Jr., He Z, Grignon DJ, Cher ML. Severe combined immunodeficient-hu model of human prostate cancer metastasis to human bone. Cancer Res 1999;59:1987-93.

[8] Yonou H, Yokose T, Kamijo T, Kanomata N, Hasebe T, Nagai K, et al. Establishment of a novel species- and tissue-specific metastasis model of human prostate cancer in humanized non-obese diabetic/severe combined immunodeficient mice engrafted with human adult lung and bone. Cancer Res 2001;61:2177-82.

[9] Kuperwasser C, Dessain S, Bierbaum BE, Garnet D, Sperandio K, Gauvin GP, et al. A mouse model of human breast cancer metastasis to human bone. Cancer Res 2005;65:6130-8.

[10] Shtivelman E, Namikawa R. Species-specific metastasis of human tumor cells in the severe combined immunodeficiency mouse engrafted with human tissue. Proc Natl Acad Sci U S A 1995;92:4661-5.

[11] Hutmacher DW, Loessner D, Rizzi S, Kaplan DL, Mooney DJ, Clements JA. Can tissue engineering concepts advance tumor biology research? Trends Biotechnol 2010;28:125-33.

[12] Lee J, Li M, Milwid J, Dunham J, Vinegoni C, Gorbatov R, et al. Implantable microenvironments to attract hematopoietic stem/cancer cells. Proc Natl Acad Sci U S A 2012;109:19638-43.

[13] Chan CK, Chen CC, Luppen CA, Kim JB, DeBoer AT, Wei K, et al. Endochondral ossification is required for haematopoietic stem-cell niche formation. Nature 2009;457:490-4.

[14] Rosen V. BMP2 signaling in bone development and repair. Cytokine Growth Factor Rev 2009;20:475-80.

[15] Reddi AH. Bone morphogenetic proteins: from basic science to clinical applications. J Bone Joint Surg Am 2001;83-A Suppl 1:S1-6.

[16] Bessa PC, Casal M, Reis RL. Bone morphogenetic proteins in tissue engineering: the road from laboratory to clinic, part II (BMP delivery). J Tissue Eng Regen Med 2008;2:81-96.

[17] Paget S. The distribution of secondary growths in cancer of the breast. Lancet 1889;133:571-3.

[18] Muller A, Homey B, Soto H, Ge N, Catron D, Buchanan ME, et al. Involvement of chemokine receptors in breast cancer metastasis. Nature 2001;410:50-6.

[19] Taichman RS, Cooper C, Keller ET, Pienta KJ, Taichman NS, McCauley LK. Use of the stromal cell-derived factor-1/CXCR4 pathway in prostate cancer metastasis to bone. Cancer Res 2002;62:1832-7.

[20] Mishra A, Shiozawa Y, Pienta KJ, Taichman RS. Homing of cancer cells to the bone. Cancer Microenviron 2011;4:221-35.

[21] Shiozawa Y, Pienta KJ, Taichman RS. Hematopoietic stem cell niche is a potential therapeutic target for bone metastatic tumors. Clin Cancer Res 2011;17:5553-8.

[22] Weilbaecher KN, Guise TA, McCauley LK. Cancer to bone: a fatal attraction. Nat Rev Cancer 2011;11:411-25.

[23] Rockwood DN, Preda RC, Yucel T, Wang X, Lovett ML, Kaplan DL. Materials fabrication from Bombyx mori silk fibroin. Nat Protoc 2011;6:1612-31.

[24] Arguello F, Baggs RB, Frantz CN. A murine model of experimental metastasis to bone and bone marrow. Cancer Res 1988;48:6876-81.

[25] Goldstein RH, Reagan MR, Anderson K, Kaplan DL, Rosenblatt M. Human bone marrow-derived MSCs can home to orthotopic breast cancer tumors and promote bone metastasis. Cancer Res 2010;70:10044-50.

[26] Seib FP, Kaplan DL. Doxorubicin-loaded silk films: drug-silk interactions and in vivo performance in human orthotopic breast cancer. Biomaterials 2012;33:8442-50.

[27] Kim UJ, Park J, Kim HJ, Wada M, Kaplan DL. Three-dimensional aqueous-derived biomaterial scaffolds from silk fibroin. Biomaterials 2005;26:2775-85.

[28] Wang Y, Rudym DD, Walsh A, Abrahamsen L, Kim HJ, Kim HS, et al. In vivo degradation of three-dimensional silk fibroin scaffolds. Biomaterials 2008;29:3415-28.

[29] Karageorgiou V, Tomkins M, Fajardo R, Meinel L, Snyder B, Wade K, et al. Porous silk fibroin 3-D scaffolds for delivery of bone morphogenetic protein-2 in vitro and in vivo. J Biomed Mater Res A 2006;78:324-34.

[30] Reddi AH, Huggins CB. Formation of bone marrow in fibroblast-transformation ossicles. Proc Natl Acad Sci U S A 1975;72:2212-6.

[31] Rentala S, Mangamoori LN. Isolation, characterization and mobilization of prostate cancer tissue derived CD133+ MDR1+ cells. J Stem Cells 2010;5:75-81.

[32] Kasoju N, Bora U. Silk fibroin in tissue engineering. Adv Healthc Mater 2012;1:393-412.

[33] Omenetto FG, Kaplan DL. New opportunities for an ancient material. Science 2010;329:528-31.

[34] Lo Celso C, Lin CP, Scadden DT. In vivo imaging of transplanted hematopoietic stem and progenitor cells in mouse calvarium bone marrow. Nat Protoc 2011;6:1-14.

**Figure Legends**

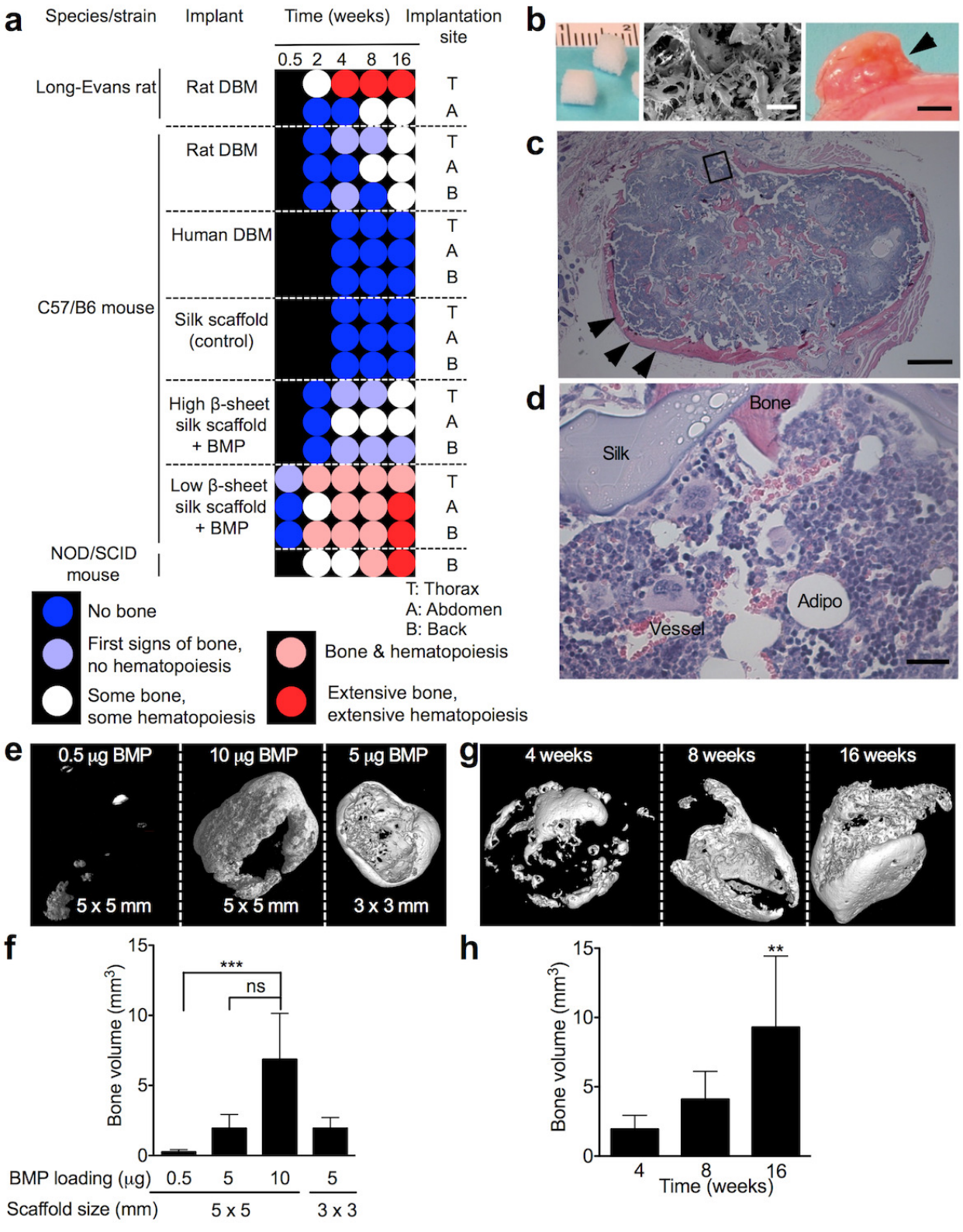


**Figure 1.** *In vivo* tissue engineered bone marrow. (**a**) Process optimization led to robust tissue-engineered bone and marrow. All silk scaffolds were 125 $mm^3$ and had a nominal BMP-2 loading

of 5 μg, except control scaffold that contained no BMP-2. Rat demineralized bone matrix (DBM) from Long-Evans rats was used as a control [30]. (**b**) Macroscopic and scanning electron microscopy images (scale bar 200 μm) of scaffolds before and after 16 weeks *in vivo*. **(c)** Corresponding H&E histology of scaffold with extensive bone (arrows) and hematopoiesis (scale bar 500 μm). Magnified area is shown in (**d**) with sinusoidal blood vessels, hematopoiesis, mature bone and silk scaffold (scale bar 25 μm). (**e**) X-ray microtomographic images of 125 $mm^3$ silk scaffolds with different amounts of BMP-2 after 4 weeks *in vivo* and (**f**) corresponding quantification. (**g**) Representative images and (**h**) bone volume measurements for 125 $mm^3$ scaffolds loaded with 5 μg BMP-2 over time. (Error bars, s.d.; $^{**}P < 0.01$; $^{***}P < 0.001$; ns, not significant; $n \geq 3$).

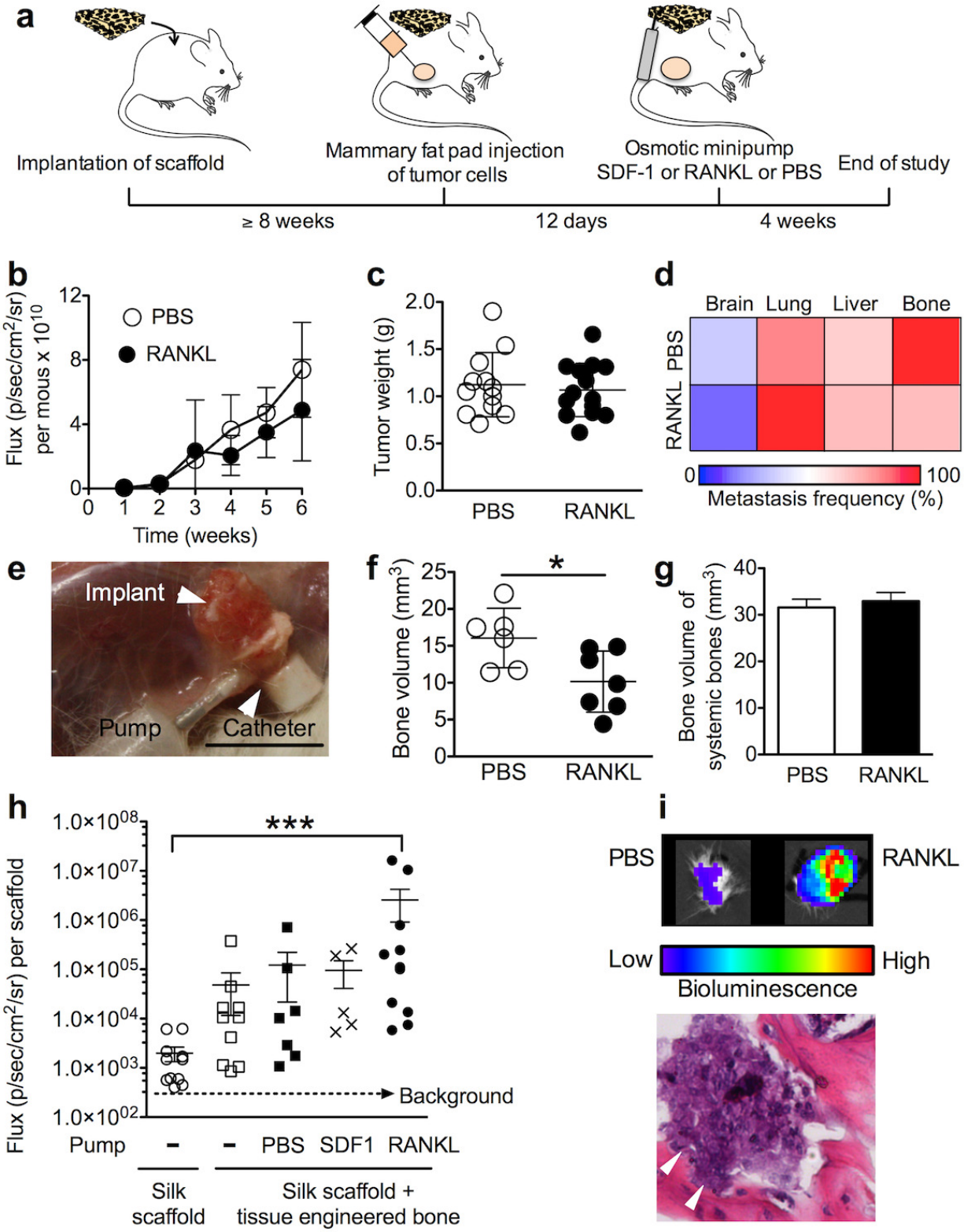


**Figure 2.** Engineering a surrogate niche for metastasizing breast cancer cells. (**a**) Experimental design for the breast cancer study. Delivery of RANKL did not impact (**b**) primary tumor growth,

(**c**) weight of the primary tumor, and (**d**) the extent of metastasis. (**e**) Image of the setup at the end of the study. (**f**) The RANKL scaffolds contained less bone as determined by X-ray microtomography, (**g**) but did not affect the bone volume of the systemic bones (femur + tibia + fibula). (**h**) Bioluminescence quantification of explanted scaffolds at the end of the study. (**i**) Bioluminescence image of scaffolds with corresponding histology of the RANKL scaffold; errors denote areas of bone resorption. (Error bars, s.d.; $*P < 0.05$; $***P < 0.001$; $n \geq 3$).

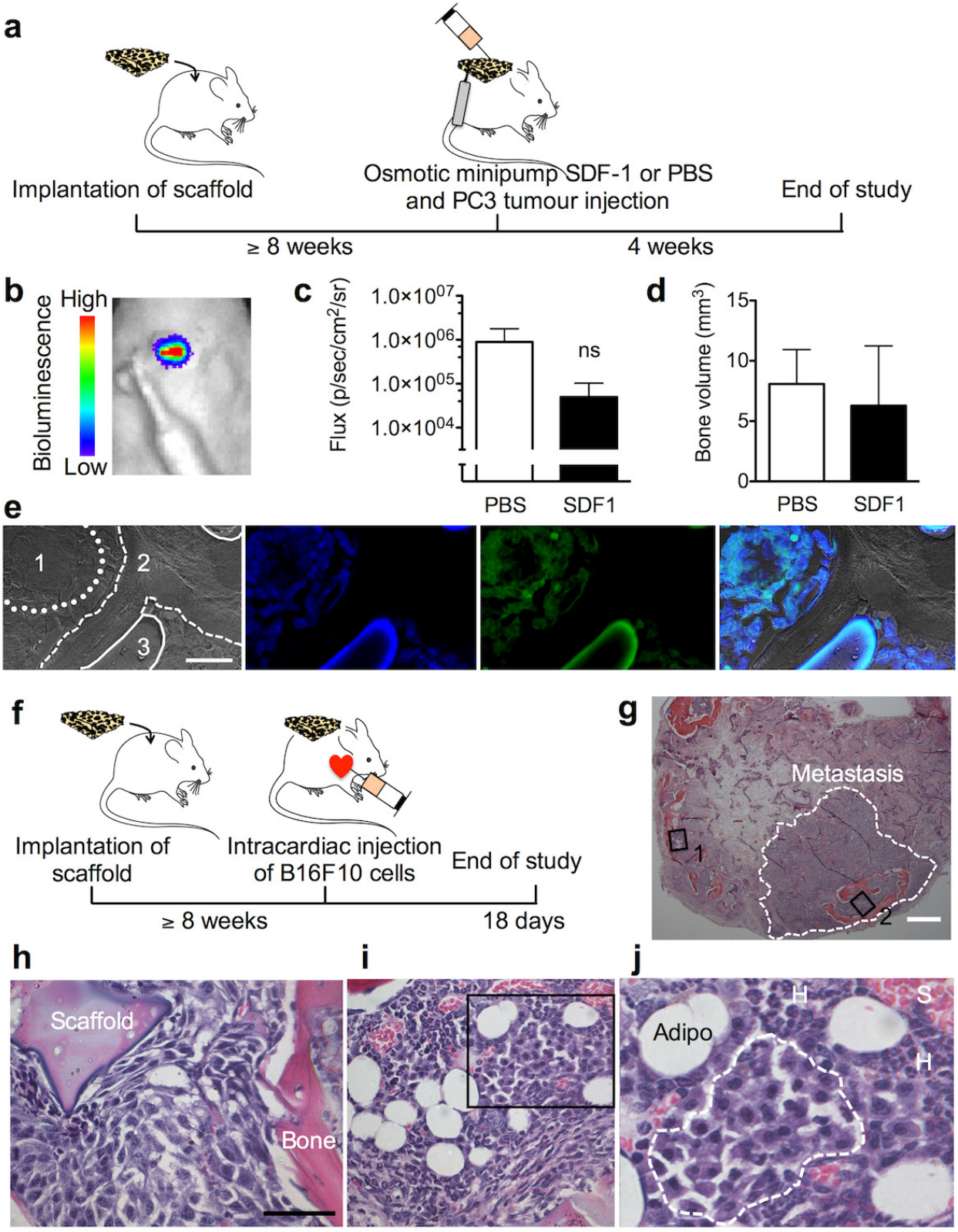


**Figure 3.** Engineered bone marrow microenvironment for prostate cancer and experimental metastasis. (**a**) Experimental design for the prostate cancer study. (**b**) *In vivo* bioluminescence image of PC3 cells in scaffold with integrated osmotic minipump and (**c**) respective quantification

of bioluminescence at week 2 (Error bars, s.d.; ns, not significant; n = 5). (**d**) Bone volume measurements of scaffolds at week 4. (**e**) Phase contrast image of (1) PC3s (dotted line), (2) tissue-engineered bone (dashed line), (3) silk scaffold (solid line) and fluorescent images corresponding to nuclei, PC3s and stacked images (scale bar 20 μm); all images were from the SDF-1 treatment group. (**f**) Design for the experimental metastasis study in immune-competent mice. (**g**) H&E histology of scaffold with macrometastasis (scale bar 400 μm). (**h**) Magnified view of area 2 and (**i**) area 1 from panel (g) (scale bar 50 μm). (**j**) Magnified view of selected area with micrometastasis (dashed line), hematopoiesis (H), sinusoidal vessels (S), and adipocytes (Adipo).

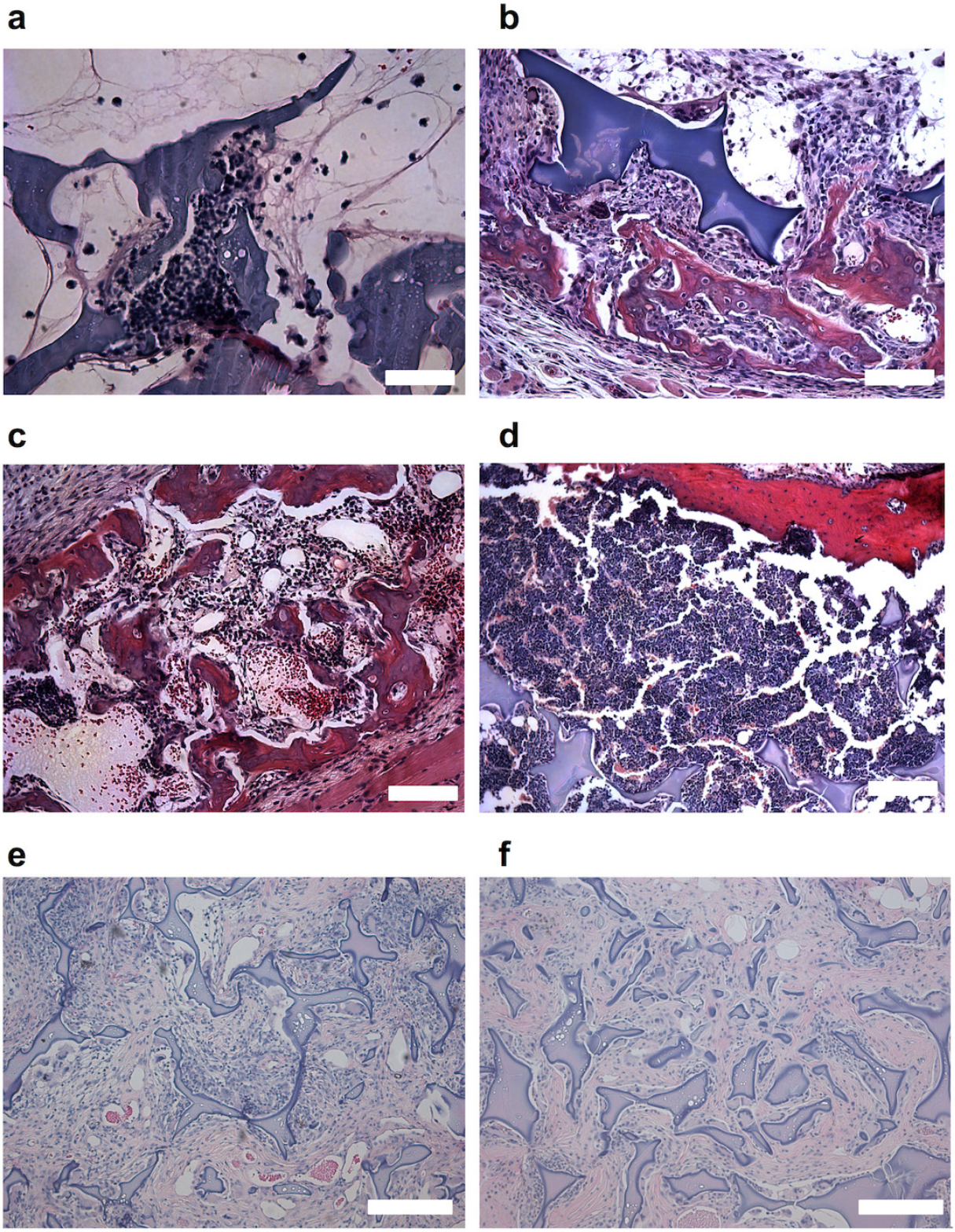


**Supplementary Figure 1.** Histology of *in vivo* tissue engineered bone marrow. Representative examples for (**a**) first signs of bone without hematopoiesis (scale bar 25 μm), (**b**) initial bone formation and marrow establishment (scale bar 50 μm), (**c**) bone and hematopoiesis (scale bar 100

μm), (**d**) extensive bone and extensive hematopoiesis (scale bar 200 μm), (**e**) no marrow at 4 and (**f**) 16 weeks (scale bars 200 μm).